Supplementary Information for

Site-specific attraction of surface colloids driven by gradients of liquid crystalline distortions

Takuya Ohzono

Contents: Figs S1-S4 and Note (in four pages)

Figure S1.

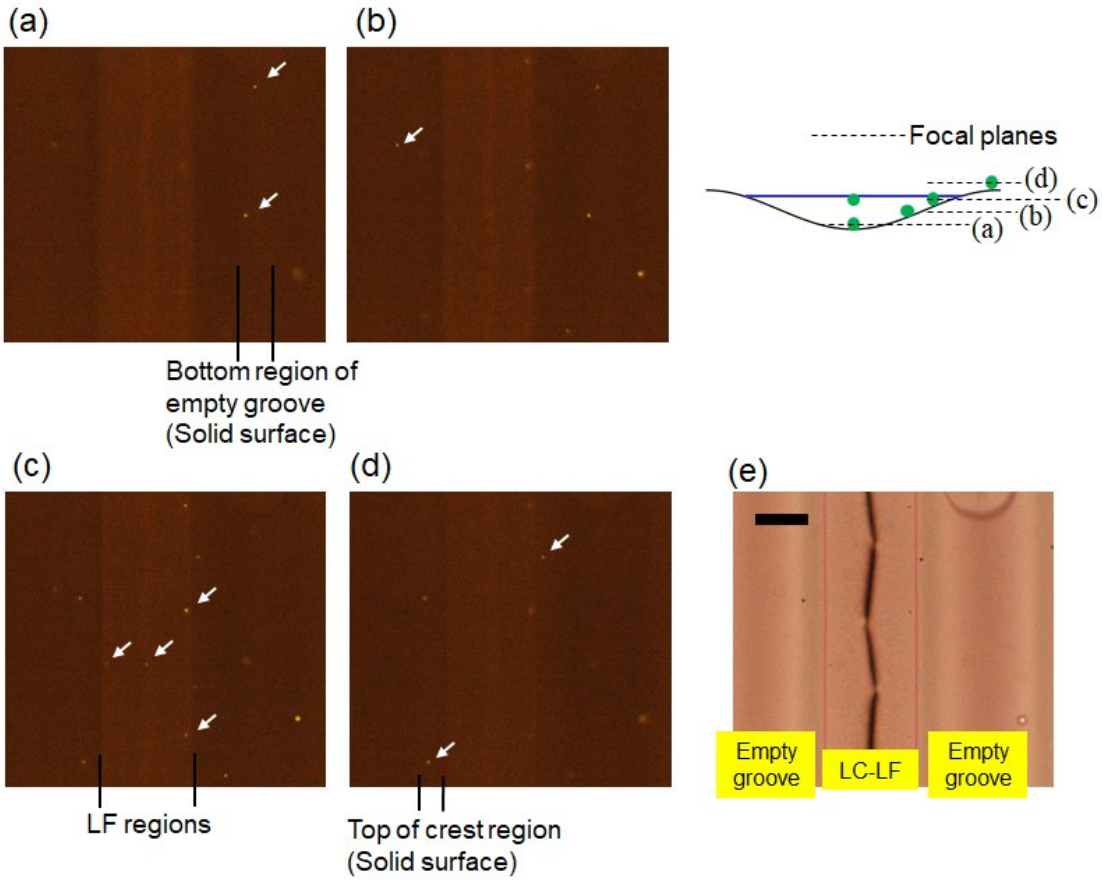

Fig. S1 FOM images acquired at different focal planes at (a) $z \sim 0$ (bottom of wrinkle grooves), (b) ~1, (c) ~2.1 (close to the air/LF interface), and (d) 2.5 μm (top of the wrinkle crests). (e) POM (parallel-nicol) image of the identical area. (Bar: 10 μm) The area with grooves filled with a LF of 5CB and the empty grooves are imaged. All the particles in the LF region on (c) are in focus and they are out of focus for the other images, suggesting that they exist at the same height close to the z-position of the air/LF interface.

Figure S2.

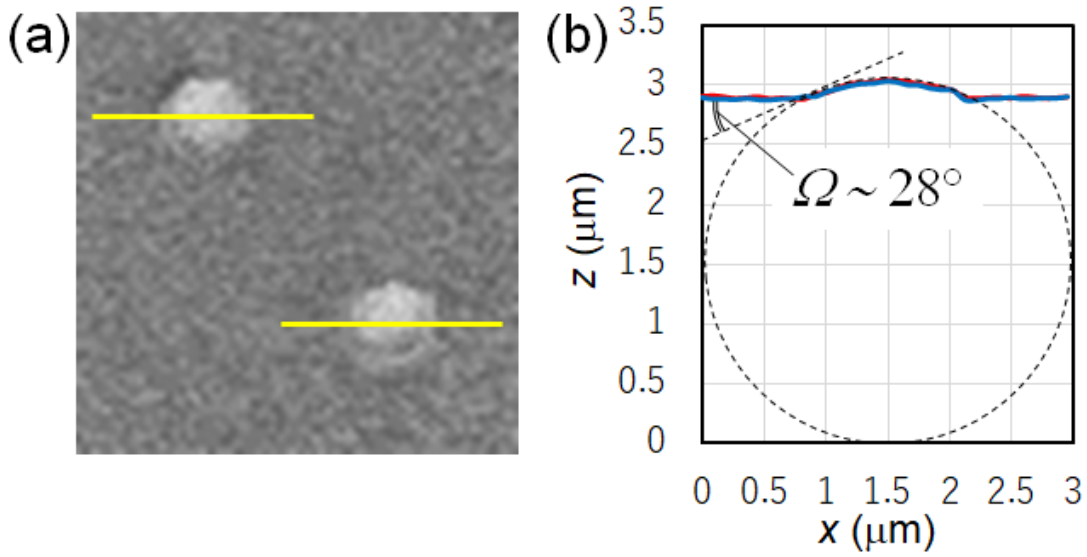

Fig. S2 (a) Confocal reflection microscopy image of larger silica particles with R~1.5 μm (FITC-labeled Scistar, Micromod) and (b) two cross-sections (bold lines) at yellow lines in (a) to estimate the contact angle Ω of 5CB at the surface of the silica particle. With a smaller particle with R~250 nm, a reliable profile data for the estimation of Ω cannot be acquired using the confocal microscope.

Figure S3.

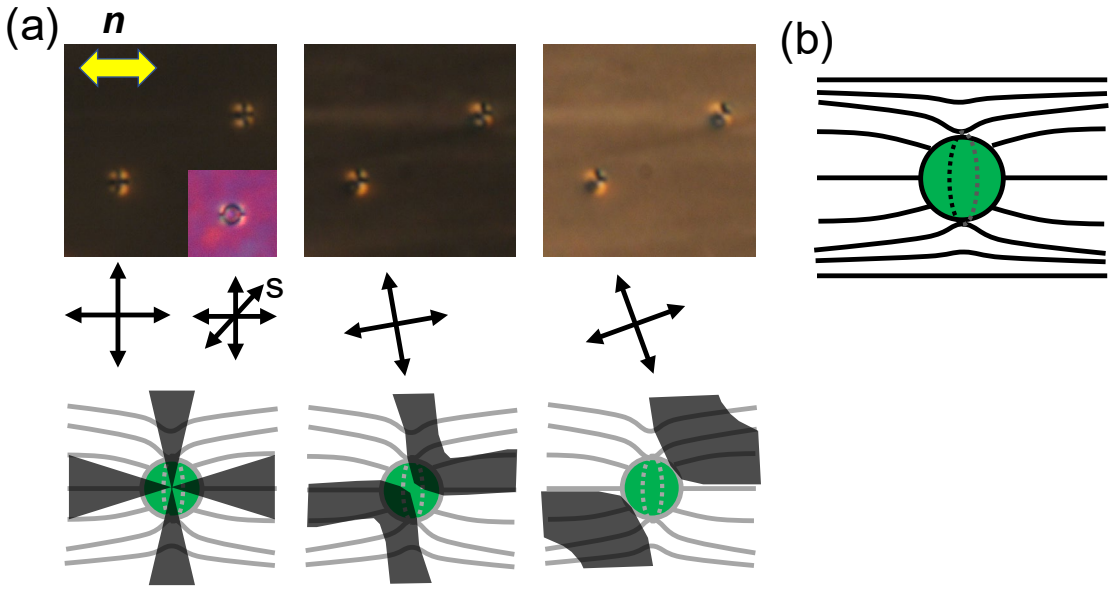

Fig. S3 (a) Polarized optical microscope images of larger silica particles with R~1.5 μm fully embedded in a planar cell (director direction is shown by a yellow arrow) for estimation of the anchoring condition of the present silica particle. Images with different angles of crossed-polarizers presented by black arrows are shown. An image with the sensitive tint plate (red plate) denoted by "S" (at slightly different focal plane to that without the sensitive tint plate) is also shown in the inset, which shows slight difference of colors depending on the quadrants; more bluish color at 1st and 3rd quadrants. The results suggest the homeotropic and weak anchoring on the present silica particles rather than the planar one generally known for the silica surfaces. (b) Estimated director configuration around the particle, represented as a Saturn ring type. The corresponding schematics of the dark regions on the images with different angles of polarizers (rotated counterclockwise) are also shown at the bottom of (a). If the anchoring were planar and boojum type alignment were formed, (i) the images shown here were observed when the crossed polarizers are rotated reversely (clockwise) (ii) the image with tint plate would show more yellowish color at 1st and 3rd quadrants.

Figure S4.

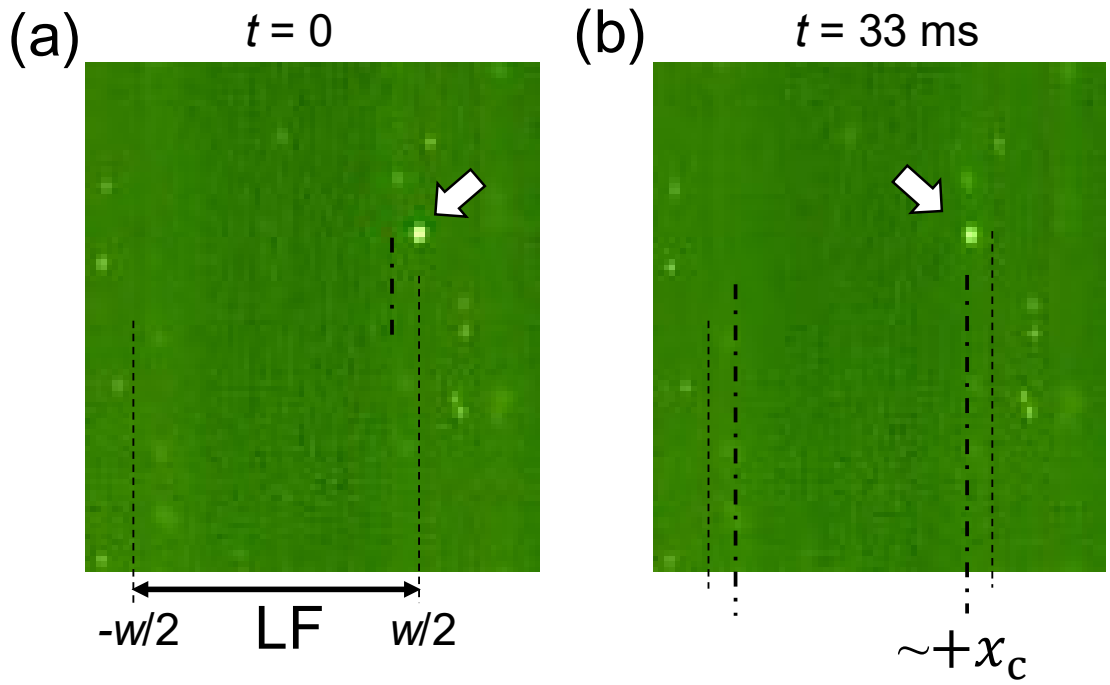

Fig. S4 (a) Typical FOM images of a particle (indicated by arrows) after reaching the furthermost ends, $|x_i| \sim w/2$, and (b) is quickly drawn to $\sim \pm x_c$ within ~33 ms.

Supplementary Information Note. Corrections to potential energy $U_{\mathrm{R}}(x)$ for wedge region by taking finite anchoring strength of air-LC interface into account.

Although the top air/LC interface imposes the homeotropic alignment, $\Delta\varphi = 0$, the actual angle at the interface may deviate from this condition because $\Delta\varphi \neq 0$ due to a finite anchoring energy $\frac{1}{2}W(\Delta\varphi)^2$ at the interface with $W \sim 10^{-5}$ Jm^{-2}and the hybrid alignment in the present system (see right Figure).

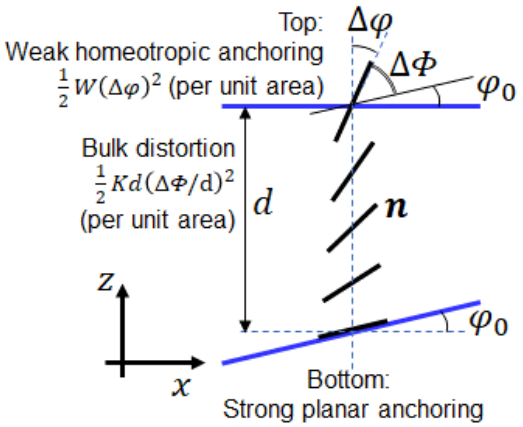

Since the anchoring strength at the planar alignment at the bottom is one-order larger than that of the top, it is assumed to be infinitely large for simplicity. An approximate value for the minimized $\Delta\varphi$ can be obtained by minimizing the total energy per unit area $\frac{1}{2}W(\Delta\varphi)^2 + \frac{1}{2}Kd(\Delta\Phi/d)^2$, leading to $W(\Delta\varphi) + K(\Delta\Phi/d)\frac{\partial(\Delta\Phi)}{\partial(\Delta\varphi)} = 0$ [2]. The optimized deviation angle is obtained as $(\Delta\varphi)^* = \frac{1}{d(W/K)+1}\left(\frac{\pi}{2} - \varphi_0\right) = \frac{1}{d/\xi+1}\left(\frac{\pi}{2} - \varphi_0\right)$, where $\xi = \frac{K}{W}$ is the extrapolation length. The optimized expression is given as $(\Delta\Phi)^* = \frac{\pi}{2} - \left\{\frac{1}{d/\xi+1}\left(\frac{\pi}{2} - \varphi_0\right)\right\} - \varphi_0 = \left(\frac{d}{d+\xi}\right)\left(\frac{\pi}{2} - \varphi_0\right)$.

We should then reconsider the energy gain with respect to the replacement with the particle. The top interface stores some energy $\frac{1}{2}W(\Delta\varphi)^{*2}$ by decreasing the bulk splay-bend distortions and a part of this surface energy is also removed upon particle replacement. Thus, U_{R} is corrected by adding the surface term as $U_{\mathrm{RW}} = U_{\mathrm{RB}} + U_{\mathrm{RS}} = -\frac{V_{\mathrm{e}}}{2}K(\nabla\theta)^{*2} - \frac{a_{\mathrm{e}}}{2}W(\Delta\varphi)^{*2}$, where a_{e} is the replaced interface area $\sim\pi R^2\cos^2\Omega$. As a result, $U_{\mathrm{RW}} = -\frac{1}{2}\frac{K}{(d+\xi)^2}\left(\frac{\pi}{2} - \varphi_0\right)^2 (V_{\mathrm{e}} + a_{\mathrm{e}}\xi)$, where d is the only function of x.

Recalling that $U_{\mathrm{R}} \approx -\frac{V_{\mathrm{e}}}{2}K\left(\frac{\frac{\pi}{2}-\varphi_0}{d}\right)^2$ by neglecting the weak dependence of $\boldsymbol{n}$ on x, the dimensionless correction factor $C[d(x)]$ defined by $U_{\mathrm{RW}} = U_{\mathrm{R}}C[d(x)]$ leads to $C\big(d(x)\big) = \left(\frac{a_{\mathrm{e}}}{V_{\mathrm{e}}}\xi + 1\right)\Big/\left(1 + \frac{\xi}{d}\right)^2$, which is plotted with respect to x in the figure on the bottom right. This indicates that the potential depth U_{R} would decrease down to $C(x)U_{\mathrm{R}}(x)$ and the correction becomes larger as the x position moves close to the edge. For example, at $x \approx x_{\mathrm{c}} \approx 7.2$ μm, $C \approx 0.3$. Then, the potential depth $U_{\mathrm{R}}(x_{\mathrm{d}}) - U_{\mathrm{R}}(x_{\mathrm{c}})$ may be corrected leading to $C(x_{\mathrm{d}})U_{\mathrm{R}}(x_{\mathrm{d}}) - C(x_{\mathrm{c}})U_{\mathrm{R}}(x_{\mathrm{c}}) \approx 100k_{\mathrm{B}}T$, which is approximately one-third of the originally calculated value without the effect of finite anchoring at the top interface.